Journal of Hydrology 594 (2021) 125750

Contents lists available at ScienceDirect

Journal of Hydrology

journal homepage: www.elsevier.com/locate/jhydrol

Research papers

Hydrodynamics and sediment deposition in turbidity currents: Comparing continuous and patchy vegetation canopies, and the effects of water depth

Marianna Soler [a,*], Teresa Serra [a], Andrew Folkard [b], Jordi Colomer [a]

[a] Department of Physics, University of Girona, Girona, Spain
[b] Lancaster Environment Centre, Lancaster University, Lancaster, United Kingdom

ARTICLE INFO

This manuscript was handled by Marco Borga, Editor-in-Chief, with the assistance of Juan Francesco Comiti, Associate Editor

Keywords:
Turbidity current
Vegetation canopy
Patch length
Sedimentation
Hydrodynamics

ABSTRACT

A flume experiment was carried out to improve understanding of interactions between turbidity currents and aquatic vegetation canopies and their landscape-scale consequences. It focussed on comparing hydrodynamics and sediment deposition in continuous canopies with those in vegetation patches, and on the effects of varying water depth – both of which are previously unreported. The currents' particulate load was characterised as a mix of fine and coarse fractions. Varying canopy frontal densities, a, and water depths, H, were used. Fifteen runs were carried out with the flume fully vegetated, and a further ten with shorter vegetation patches. In all runs, the currents evolved as expected through inertial, drag-dominated and viscous regimes. The positions at which transitions between the regimes occurred were measured and analysed. In the fully-vegetated runs, both transition positions varied linearly with aH for $aH < 0.8$, and were constant when $aH > 0.8$. We argue that the variation at lower values of aH is caused by non-canopy drag forces becoming non-negligible compared to the canopy drag. An equation is derived that models, as a function of a and H, the size a vegetation patch needs to be for its effect on turbidity currents to be the same as that of a continuous canopy. The sediment depositional flux rate for fine particles from the currents within the vegetation was greater than that for coarse particles, by a factor of 1.57. This suggests that bed sediment deposited within canopy patches by turbidity currents will be on average finer than that in gaps between patches, as has been found previously for currents and waves. Thus, this effect will contribute to the development of inter-tidal and shallow sub-tidal landscapes characterized by patches of dense vegetation and fine sediments, surrounded by bare regions with coarser sediments. Our results imply that the distances over which the phenomena we document occur in typical inter-tidal and shallow sub-tidal contexts are of the same order of magnitude as sizes of patches of saltmarsh plants and seagrasses. This indicates that the reported patch length effects are highly relevant to understanding eco-hydrological interactions in these contexts.

1. Introduction

1.1. Biophysical interactions in aquatic plant canopies

The effects of aquatic plant canopies on hydrodynamic, sedimentary and geomorphological processes have been studied in many contexts, including seagrass meadows (e.g. Agawin and Duarte, 2002; Folkard, 2005; El Allaoui et al., 2016; Colomer et al., 2017); mangroves (e.g. Nardin et al., 2016; Gillis et al., 2019); saltmarshes (e.g. Adam, 2002; Schulze et al., 2019); in-stream and riparian river vegetation (e.g. Cotton et al., 2006; Curran and Hession, 2013; Gurnell, 2014; Licci et al., 2019; Lowe et al., 2010; Montakhab et al., 2012); and in more general or idealized studies (e.g. Nepf, 1999; Madsen et al., 2001; Zong and Nepf, 2010; Liu and Nepf, 2015; Manners et al., 2015; Zhang et al., 2018). They have been found widely to act as ecosystem engineers (e.g. Ludwig et al., 2005; Nepf, 2012), modifying landscape evolution via biophysical interactions at multiple scales (Folkard, 2019). In addition, macrofauna living in submerged coastal environments, actively interact with plant canopies to the point of controlling resuspension, and therefore erodibility and sediment distribution (Joensuu et al., 2018). Understanding these interactions and their consequences is therefore crucial for understanding the functioning of coasts, lakes and rivers.

* Corresponding author.
E-mail addresses: marianna.soler@udg.edu (M. Soler), teresa.serra@udg.edu (T. Serra), a.folkard@lancaster.ac.uk (A. Folkard), jordi.colomer@udg.edu (J. Colomer).

https://doi.org/10.1016/j.jhydrol.2020.125750
Received 8 May 2020; Received in revised form 26 September 2020; Accepted 6 November 2020
Available online 18 November 2020

In recent years, because of climate change and other anthropogenic stresses, aquatic plant canopies have become increasingly degraded, through either fragmentation (Adam, 2002; Tamburello et al., 2012) or reduction of the area they cover (Richardson et al., 2007; Colomer et al., 2017; Dwirea et al., 2018; Serra et al., 2018; Xiu et al., 2019). For this reason, research into their biophysical interactions has recently focussed on fragmented and finite-sized canopies (Bouma et al., 2007; Zong and Nepf, 2010; El Allaoui et al., 2015, 2016; Zhang et al., 2018).

Most studies of biophysical interactions of fragmented aquatic vegetation canopies have considered their interactions with uni-directional flows. In this context, one of the main ways in which vegetation canopies engineer their physical environment is through reducing bed erosion (Madsen et al., 2001) and increasing deposition of sediment (Agawin and Duarte, 2002; Montakhab et al., 2012; Zong and Nepf, 2010). This triggers a positive feedback, as retention of fine sediment - which is rich in organic material and nutrients - by the vegetation promotes the expansion of the vegetated region (Gurnell, 2014). A minimum patch size and minimum stem density within a patch of vegetation is required for it to have the capability to engineer its physical environment in this way (Licci et al., 2019), and to produce a positive feedback for the vegetation (Bouma et al., 2009). Deposition of sediment within vegetation canopies is dependent on the mean flow speed and the characteristics of the vegetation (Liu and Nepf 2015). Hence, as well as completely fragmented canopies having sediment dynamics that are dependent on their spatial structure, this is also the case in continuous canopies in which plant properties such as stem diameter, flexibility and density are spatially heterogeneous (e.g. Schulze et al., 2019). Thus, the hydrodynamics of heterogeneous canopies depend on variations of canopy characteristics at both the patch- and meadow-scale (Adhitya et al., 2014).

The interactions of vegetation canopies and uni-directional flows may also produce negative feedbacks, for example when the enhancement of flow speed adjacent to lateral patch edges produces scouring which inhibits plant growth and patch development (Schoelynck et al., 2012; Bouma et al., 2013). Differences in patch diameter, inter-patch distances and plant densities have been found to produce differences in velocity flow structures around patches. For example, both the amount of flow acceleration around patches and the lateral distance from the patch to the point where maximum flow acceleration occurs increase with increasing patch size (Vandenbruwaene et al., 2011).

The presence of scale-dependent feedbacks such as these create self-organised heterogeneity in landscapes and are key mechanisms responsible for shifts between unvegetated and vegetated landscape states (Bouma et al., 2009). They have important implications for ecosystem functioning, such as increased ecosystem productivity and increased resilience and resistance to environmental change (Rietkerk and van de Koppel, 2008).

El Allaoui et al. (2015), El Allaoui et al. (2016) and Colomer et al. (2017) extended studies of hydrodynamic interactions with heterogeneous vegetation canopies in oscillating flows. As with the work cited above, they found that the spatial scale of variations (patch and gap size) and canopy characteristics (stem density) to be the most important factors determining wave transformations, levels of turbulent kinetic energy and therefore sediment dynamics. In particular, El Allaoui et al. (2015) and Colomer et al. (2017) studied the hydrodynamics in gaps aligned with the direction of the wave and found that the lateral vegetation altered the gap for distances below 1.5 h_v (being h_v the vegetation height). El Allaoui et al. (2016) studied the hydrodynamics in gaps situated perpendicular to the direction of the wave. They found a greater sheltering for gaps surrounded by denser canopies and for smaller gaps.

To date, there has been little work on biophysical interactions between heterogeneous or fragmented vegetation canopies and a third hydrodynamic phenomenon (beyond the uni-directional currents and waves discussed above), namely gravity currents. In the context of considering canopies' effects on sediment dynamics and thus the sort of feedbacks described, the most pertinent forms of gravity currents are those driven by suspended particle concentration, namely turbidity currents. Soler et al. (2017, 2020)) considered the interactions of turbidity currents with continuous, uniform vegetation canopies and the effects of varying turbidity current particulate concentration, canopy density and vegetation type, indicating that turbidity currents were able to retain sufficient sediment in suspension to maintain their flow until they became significantly influenced by the drag exerted by the obstacles, Furthermore, they found that while turbidity current was flowing in the drag dominated regime, the deposited material became increasingly dominated by fine sediment, at a rate dependent on the vegetation type, starting this transition at a distance equivalent to 5.1–7.6 times the total water depth; Barcelona et al. (2018) considered the interaction of turbidity currents with longitudinal patches, i.e. patches of vegetation aligned with the direction of the propagation of the turbidity current, in order to find the effect of longitudinal gap size on gravity current evolution and on the sedimentary rates. Their studies indicated that a critical canopy volume lower than 0.025, was required to produce significant changes in hydrodynamics and sedimentation rates. Here, we extend this work by investigating for the first time the effects of water depth on turbidity current-vegetation patch interactions, and the hydrodynamics and sediment deposition patterns of turbidity currents in finite-length transversal patches of vegetation, i.e. patches of vegetation oriented perpendicular to the direction of the turbidity current development.

1.2. Gravity current hydrodynamics

Gravity current hydrodynamics have been studied for many years both theoretically (Benjamin, 1968) and experimentally (Simpson, 1982; Shin et al., 2004). The most common approach used in experimental studies has been lock-exchange flume experiments, in which two fluids of different densities (usually generated by salt dissolution) are initially at rest in a flume and separated from each other by a lock gate. When the gate is removed, differences in the hydrostatic pressure cause the denser fluid to flow as a gravity current beneath the less-dense fluid, along the bottom boundary of the flume, forcing the less-dense fluid to flow in the opposite direction over the denser fluid. As the gravity current flows along the flume, it passes through three regimes (e.g. Huppert and Simpson, 1980; Maxworthy et al., 2002), see Table 1. In the first – known as the 'inertial regime' – the current proceeds as if released from an infinite reservoir, and the position of the front of the current (hereinafter referred to as the 'current toe', following Tanino et al., 2005), x_c, varies in direct proportion to time, t, and depends on the reduced gravity, g', and water depth, H (Tanino et al., 2005). When the lock gate is removed, it generates an interfacial wave that propagates in the opposite direction to the gravity current until it reflects off the back wall of the flume. This reflected wave then flows in the same direction as the gravity current and at the point it catches up with the current toe, the second regime begins. In this 'self-similar regime', the current motion is determined by a balance between buoyancy and inertial forces, and the flow slows over time such that the position of the toe varies as $t^{2/3}$ (Maxworthy et al. 2002). However, if the current is propagating through an array of obstacles (for example, simulated or natural vegetation), it evolves instead from the inertial regime to a 'drag-dominated regime' (e.g. Tanino et al., 2005; La Rocca et al., 2008; Zhang and Nepf, 2008, 2011; Gonzalez-Juez et al., 2010; Nogueira et al., 2013, 2014; Bhaganagar, 2014; Soler et al., 2017, 2020). Here, the gravity current is affected by the drag due to the obstacles, which dominates over both inertial forces and the drag forces caused by the flume bed and sidewalls. In this regime, the speed of the current toe reduces more than in the self-similar regime found in obstacle-free cases, varying from $x_c \propto t^{2/3}$ to $x_c \propto t^{1/2}$ (Hatcher et al., 2000).

In order to quantify the drag forces due to an array of obstacles, it is necessary to calculate its drag coefficient, C_{Da}. For randomly-distributed arrays of vertical cylinders (often used to simulate plant stems), Ghisalberti and Nepf (2004) found that

Table 1
Summary of gravity current hydrodynamics, showing the time dependency of the position of the current toe, x_c, depending on the density-varying agent and the existence or absence of obstacles.

	Density varying agent	volume release	Regime		
			Inertial	Self-similar	Viscous
Without obstacles	conservative (heat, salinity)	Infinite Finite	$x_c \sim t^1$	$x_c \sim t^{1/2}$	$x_c \sim t^{1/5}$
	Not conservative (particles suspension)	Finite		$x_c \sim t^{2/3}$	
			Inertial	Drag-dominated	Viscous
With obstacles	Conservative (heat, salinity)	Finite	$x_c \sim t^1$	$x_c \sim t^{1/2}$	$x_c \sim t^{1/5}$
	Not conservative (particles suspension)	Finite		$x_c \sim t^{1/2}$	

$$C_{Da} = C_D/1.16\left\{1.16 - 9.31ad + 38.6(ad)^2 - 59.8(ad)^3\right\} \quad (1)$$

where $a = Nd/A$ is the frontal area of the cylinders per unit volume (Nepf, 1999), N is the number of stems, d is stem diameter and A is the bed area over which the N stems are distributed. C_D is the drag coefficient associated with the individual obstacles (which are assumed to be cylinders), and is a function of the cylinder Reynolds number $Re_c = ud/\nu$, where ν is the kinematic viscosity of the fluid, and u the speed of the current toe, such that $C_D = 1 + 10Re_c^{-2/3}$ (White, 1991). This expression for C_D applies for Re_c values ranging from 1 to 10^5 and dimensionless array densities $ad < 0.03$ (Nepf, 1999). Note that this implies that the drag coefficient of a randomly-distributed array of obstacles in a flume will increase as a gravity current travels along the flume due to the reduction in the velocity of the gravity current.

The third and last regime through which gravity currents pass is called the 'viscous regime' and occurs when the current has spread so far that it has become thin enough for viscous forces between the two fluids to become important and overcome the inertial forces. In this regime, the speed of the current toe reduces until its position varies as $x_c \sim t^{1/5}$.

1.3. Turbidity currents

Turbidity currents are gravity currents in which the density-varying agent is the concentration of particles in suspension. Their dynamics can be more complicated than those of gravity currents in which the density-varying agent is conservative on the timescale of the current's development, for example heat or salt concentration. This is because of sediment loss due to deposition and/or sediment entrainment due to bed scouring, which change the density difference that drives the current, altering its temporal evolution (Francisco et al., 2017). Bonnecaze et al. (1993) found that the position of the toe of a turbidity current of finite volume spreading over a rigid, unobstructed horizontal surface in shallow water, evolved following $x_c \propto t^{2/3}$ (Table 1). The spatial and temporal evolution of turbidity currents is dependent on their grain-size distribution, that is, the ratio between the amounts of fine and coarse particle they carry (Felix 2002). Currents dominated by fine particles travel over larger distances, which results in sedimentation further downstream than in currents dominated by coarse particles (Harris et al., 2002). Moreover, the runout distance to which coarse particles are transported by turbidity currents increases substantially when the proportion of fines in the turbidity current is increased (Gladstone et al., 1998).

In natural environments, turbidity currents are often observed travelling, or to have travelled, through arrays of obstacles. One example of this is turbidity currents flowing through aquatic vegetation canopies. In experiments investigating this configuration, Soler et al. (2017) found that the controlling factor in the temporal evolution of the current toe position was the canopy drag. They also compared their results to experiments studying a salinity-driven gravity current passing through an array of obstacles (Hatcher et al., 2000) and found that, although $x_c \propto t^{1/2}$ in both cases, the effect of depositional loss of sediment particles from the turbidity current was a reduction of 70% in the constant of proportionality in this relationship.

Coastal areas of aquatic vegetation, which are subject to ever-increasing anthropic pressures, have become heavily degraded, resulting in their fragmentation (Folkard, 2019), creating a mosaic of vegetation and bare soil areas. The presence of patches also produces wakes that can affect patches situated downstream (Folkard, 2005, 2019). Taking into account the engineering capability of vegetation, which modifies the hydrodynamics within its surroundings, it is expected that the patch length scale plays a critical role in the development of the turbidity currents within vegetation patches and downstream.

As noted above, studies of turbidity currents' interactions with arrays of obstacles or vegetation canopies to date have focussed on cases where the array or canopy is continuous and uniform. Cases where the vegetation canopy is of finite extent have not previously been considered. This leaves open the questions of how the size of finite patches affects their influence on turbidity current hydrodynamics and sediment transport processes, and specifically how long vegetated patches need to be to provide dynamic effects equivalent to those of continuous vegetated canopies – the equivalent question to that addressed by Licci et al. (2019) for vegetation patches in uni-directional flows in rivers. These questions are addressed in the present study, by measuring the effects on current hydrodynamics and sediment deposition of vegetation patches that end at different points within the currents' evolution through the three dynamic regimes described above, and comparing them to the effects of continuous vegetation canopies.

2. Material and methods

2.1. Experimental set-up

The experiment was conducted in a methacrylate flume (4.0 m long, 0.3 m high and 0.3 m wide) that was separated into two sections with a removable vertical lock gate (Fig. 1). The shorter reservoir section was filled with a mixture of sediment and water that would create the turbidity current, while the longer section was filled with water only. The longer experimental section was populated with vertical PVC dowels with a diameter of 6 mm to mimic emergent rigid vegetation like that found in many salt marshes as *Juncus maritimus* (Harvey et al., 2009; Leonard et al., 1995; Tanino et al., 2005). To construct the model canopy, a PVC base sheet was perforated at positions selected using a random number generator, following Pujol et al. (2013), and a single dowel secured in each hole. The density of vegetation canopies (real or simulated) can be quantified using various parameters. Commonly, solid plant fraction (SPF) is used. This is defined as the percentage of the bed area occupied by vegetation stems, $SPF = 100n\pi\,(d/2)^2$, where n is the number of stems per unit bed area and d the stem diameter (Pujol et al., 2010). Here, runs were carried out with canopy density values from SPF = 1% (356 plants m^{-2}), to 4% (1424 plants m^{-2}), as well as a control run without plants (SPF = 0%). Canopy density is also quantified using $a = nd$, the canopy frontal area per unit bed area (or simply "frontal area density"), or the dimensionless array density, ad (= SPF/25p). All these parameters, for each experimental run, are shown in Table 2. Note that the values of ad varied from 0.013 (SPF 1%) to 0.051 (SPF 4%), and all

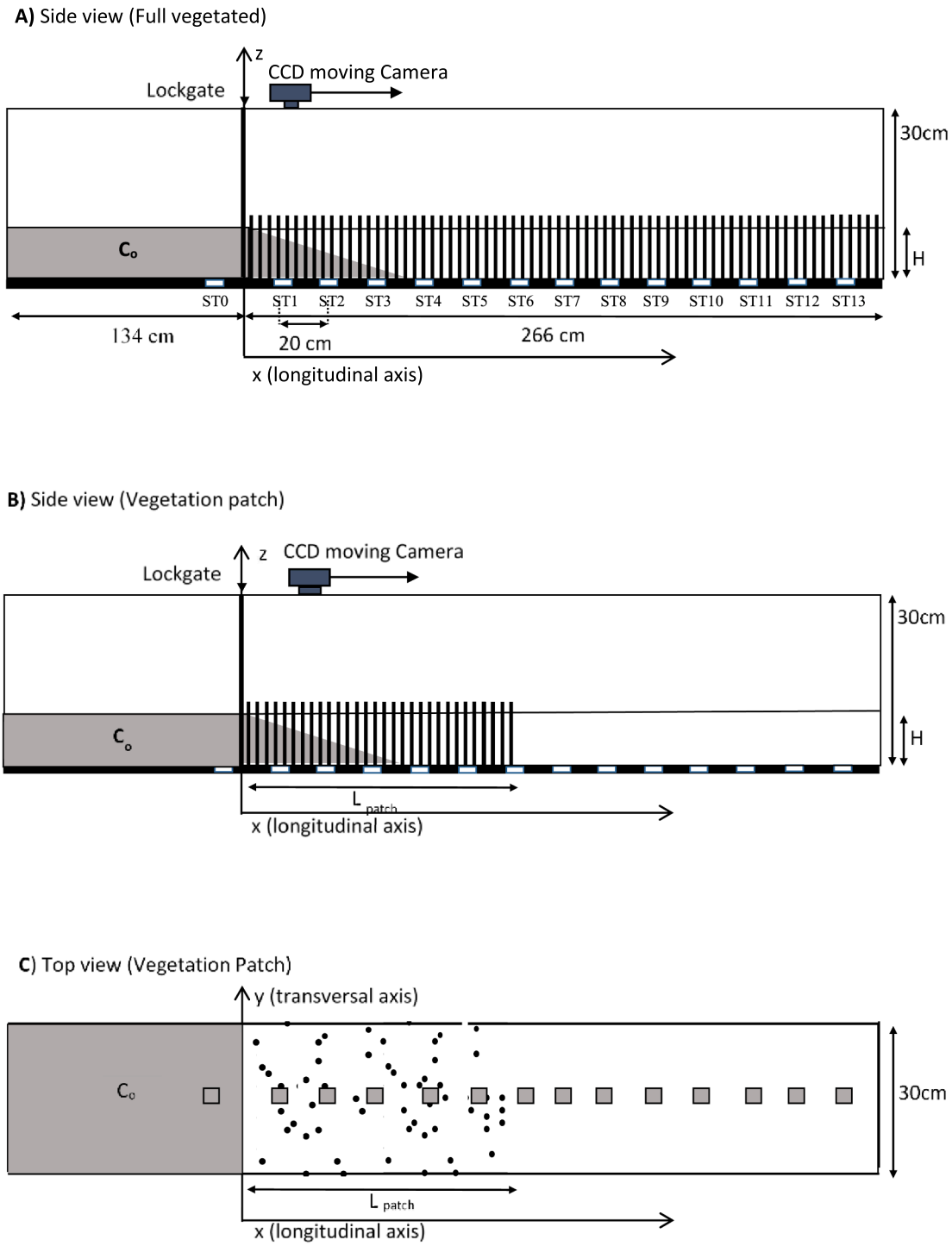

Fig. 1. (A) Side view of the laboratory flume, which is divided by a removable, sealing partition (lock gate) into two sections. The smaller, left-hand, section is a reservoir for preparation of the turbidity current fluid. The right-hand section contains the simulated vegetation and is the experimental test section. The vertical coordinate is z, with $z = 0$ at the bed (increasing upwards); the longitudinal coordinate is x, with $x = 0$ at the lock gate (increasing to the right); (B) Side view of the laboratory flume when the turbidity current (shaded) is flowing through a vegetation patch of length L_{patch}. The triangular grey area represents the interface profile of the gravity current in the drag-dominated regime; (C) Top view of the laboratory flume, with a vegetation patch in the test section, showing the locations of fourteen sediment traps (ST0 to ST13) on the flume bed. ST0 is 20 cm to the left of the lock gate, ST1 is 20 cm to the right of the lock gate, and each subsequent trap is a further 20 cm to the right. The canopy is a randomly-distributed array of obstacles with solid plant fraction (SPF) values of 1.0, 2, 2.5, 3, 3.5 and 4%.

Table 2
Summary of experimental conditions (water depth, H; vegetation density, expressed as *SPF*, a and ad; vegetation patch length, L_{patch}) and non-dimensional parameter values (vegetation frontal area, aH; canopy aspect ratio, L_{patch}/H) for each experimental run.

Full vegetated experiments						
Exp.	H (cm)	SPF (%)	Lpatch (cm)	a (m^{-1})	aH	ad
1	12	0	0	0	0	0
2		1	280 (Full)	2.13	0.26	0.013
3		2		4.20	0.50	0.025
4		2.5		5.27	0.63	0.032
5		3		6.33	0.76	0.038
6		3.5		7.40	0.89	0.044
7		4		8.47	1.02	0.051
8	15	4	280 (Full)	8.47	1.27	0.051
9	9				0.76	
10	6				0.51	
11	3				0.25	
12	15	2	280 (Full)	4.20	0.63	0.025
13	9				0.38	
14	6				0.25	
15	3				0.13	

Vegetated patchs experiments							
Exp.	H (cm)	SPF (%)	Lpatch (cm)	C_D·a·Lpatch	a (m^{-1})	aH	ad
16	6	4	116	14	8.47	0.51	0.051
17			104	12			
18			92	10			
19			77	8			
20			60	6			
21	12	4	151	14	8.47	1.02	0.051
22			132	12			
23			113	10			
24			92	8			
25			70	6			

fall within the range observed in natural vegetation canopies with $0.01 < ad < 0.1$ (Bouma et al., 2007).

2.2. Preparation of the turbidity current fluid

The flume was filled with water to a height H the day before each run to allow the water temperature to equilibrate. The lock gate was then lowered into position, separating the two sections. To generate the turbidity current, 3L of water was taken from the reservoir section (Fig. 1) in which the mass of sediment needed to produce an initial concentration of $C_0 = 6$ gL^{-1} was added, throughout the whole of the reservoir. The turbidity current concentration corresponded to 0.21% by volume, falling within the range of 0.1% to 7% categorised as low particle concentration by volume by Meiburg and Kneller (2010). The sediment–water mixture was stirred vigorously for five minutes to ensure a homogeneous sediment suspension, and then returned to the reservoir section and mixed thoroughly.

The sediment was taken from the Pletera ponds at the Empordà Marshes Natural Park in NE Spain, in order to provide natural sediment characteristics. The collected sediment was first cleaned, removing leaves and roots and then sieved to remove particles >0.5 mm. The particle size distribution of the remaining sediment was measured with a LISST-100 particle size analyser (Sequoia Scientific, Inc., Bellevue, WA, USA). It was found to have a bimodal size distribution (Fig. 2): 79.0% of the mass was made up of particles with diameters ranging from 6.2 to 104 μm (coarse fraction), 17.9% was made up of particles with diameters ranging from 2.2 to 6.2 μm (fine fraction). The coarse fraction fell into the category of weakly cohesive particles (fine to coarse silts and small sand particles) and the fine particles into the category of very cohesive particles (clays and very fine silts), according to the classification of Van Rijn (2007) and Blott and Pye (2012). The remaining 3.1% of the sediment volume consisted of only a few particles with larger volumes, which quickly settled out of the turbidity currents and therefore were not considered in the analysis.

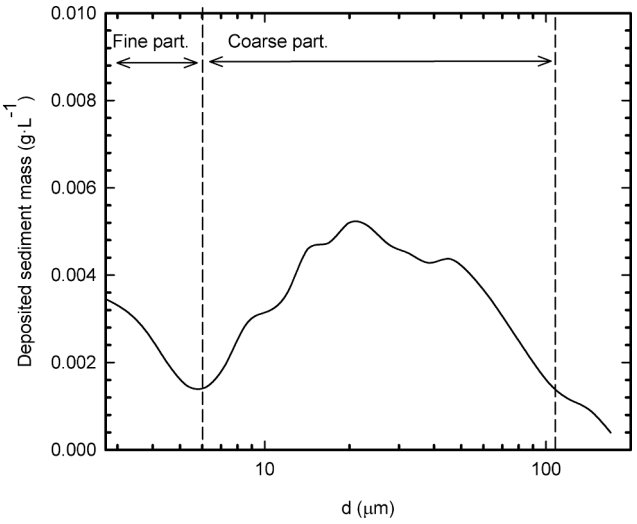

Fig. 2. Particle size distribution of the turbidity current sediments, expressed in terms of mass per unit volume (gL^{-1}). The distribution is divided into fine (2.5 μm < d < 6.2 μm) and coarse (6.2 μm < d < 104.0 μm) fractions.

2.3. Simulated vegetation patches and experimental run parameter values

Twenty-five experimental runs, all with an initial concentration $C_0 = 6.0$ gL^{-1}, were carried out, Parameter values for each run are shown in Table 2. Firstly, in addition to a control run with no vegetation (Run 1), fourteen runs (Runs 2–15) were carried out with the whole 280 cm length of the flume's experimental section populated with simulated vegetation, so that the patch length, L_{patch}, was in effect 280 cm. These were designed to investigate the influence of varying water depth and canopy density on the downstream distances at which the turbidity currents underwent the dynamic regime transitions described above, whilst they were within the vegetation canopy. Therefore, water depth and canopy density were varied from run to run, using values of $H = 3$, 6, 9, 12 and 15 cm, and SPF = 1, 2, 2.5, 3, 3.5 and 4% respectively. Subsequently, ten runs (Runs 16–25) were carried out in which the patches of simulated vegetation were shorter. In these, two water depths ($H = 6$ and 12 cm) were used, and the canopy density was held constant at SPF = 4%. The shorter patch lengths were chosen such that they ended at different points in the dynamic evolution of the turbidity current in the run in which $L_{patch} = 280$ cm, SPF = 4% and H = 12 cm (Run 7, Table 2), the maximum value of each parameter. Five different patch lengths were chosen: one which ended within the inertial regime; three ending within the drag-dominated regime; and one extending into the viscous regime.

Thus, the experimental configuration was characterized by three parameters: the vegetation canopy length, L_{patch} [m], the water depth, H [m], and the frontal area per unit volume, a [m^{-1}], which quantified the canopy density, with the turbidity current's characteristics held constant. From these, we constructed two non-dimensional parameters, which we used as the independent variables in our analyses: L_{patch}/H, the aspect ratio of the vegetation canopy; and aH ($=NdH/A$), the canopy frontal area per unit bed area. The values of these for each run are shown in Table 2. The ranges over which runs are distributed are $5.8 \leq L_{patch}/H \leq 93.3$ and $0.13 \leq aH \leq 1.27$ (and the control case, for which $L_{patch}/H = aH = 0$).

2.4. Development of the turbidity current

Once the sediment–water mixture had settled in the reservoir section

of the flume, the lock gate was released, allowing it to flow as a turbidity current into the experimental section. In all runs, the initial (inertial regime) speed of the current toe was two to three orders of magnitude greater than the settling velocity of the coarse particles, and three to four orders of magnitude higher than settling velocities of the fine particles. Thus, the current was considered to be conservative in this stage of its evolution, i.e. the density anomaly driving the current remained constant.

A moving CCD video camera was situated at the top of the flume (Fig. 1A) to determine the position and speed of the current toe. Its position, x_c, was located on the video images using edge detection (parallax error was <3% and was not corrected for) and measured on a scale with 0.1 cm gradations mounted on the flume bed. In all runs, the obscuration of the line of sight by the dowels was not enough to affect the view of the current toe. The toe speed was calculated from the position and time data recorded on the video footage of its progression down the flume. Following previous studies (Tanino et al., 2005; Soler et al., 2020) we converted the toe position into the non-dimensional parameter $C_{Da}ax_c$, and used this in our analyses of the current's hydrodynamic progression down the flume. This parameter is a measure of the drag force due to the vegetation normalized by the inertial force of the current at its toe. Hence, we refer to it hereafter as the 'normalized toe drag'.

In order to analyse the pattern of sediment deposition from the turbidity current, fourteen sediments traps (ST0 to ST13) were located along the flume bed. The first one (ST0) was located in the reservoir section, 20 cm upstream of the lock gate. The other thirteen (ST1-ST13) were evenly distributed along the flume bed at intervals of 20 cm, starting 20 cm to the right of the lock gate and finishing 10 cm from the far end of the flume. Each trap had a volume of 21.3 mL^{-1} and was inserted into the PVC base without extruding above the flume bed, to avoid any interference with the passage of the turbidity current (Fig. 1B).

When the turbidity current arrived at the end of the canopy, all the traps were covered manually with lids to avoid collection of sediment that settled out of the current after it had been reflected by the end wall. In order to avoid overestimation of the amount of sediment captured by the traps further upstream caused by the longer time of sedimentation, the effective time that each ST was collecting sediment was recorded in each run. The sediment collected in each trap was analysed with the LISST-100 (following Serra et al., 2002, 2005), which gave the volume occupied by particles in each of 32 size classes logarithmically distributed in the range 2.5–500 μm. Because the major sediment constituent in all the traps was silt particles (79%), the particle volume concentration (μL/L) was transformed into deposited sediment mass by assuming that the density of the particles was 2.798 gcm^{-3}, the standard value for silt particle density (Mandal and Maiti, 2015). No flocculation of fine sediment was observed, so its potential effects were not taken into account in this conversion. The deposited mass per unit bed area was then converted to a depositional flux at each sediment trap by dividing by the time over which the deposition occurred. This value was divided by the initial horizontal flux of sediment carried by the current as it emerged from the reservoir, giving a non-dimensional depositional flux rate, *DF*, for each trap.

3. Results

3.1. Turbidity current evolution within fully-vegetated canopies

The temporal evolution of the current toe position, x_c, in the fully-vegetated runs was dependent on the canopy density: in general, as the canopy increased, the toe speed reduced (Fig. 3). Initially in all runs (until approximately $t = 30$ s), the turbidity current was in the inertial regime, as x_c varied linearly with time (i.e. the flow speed was constant). In the non-vegetated case (SPF = 0%), after the inertial regime, the flow slowed down, taking on a time dependence $x_c \propto t^{2/3}$, while the

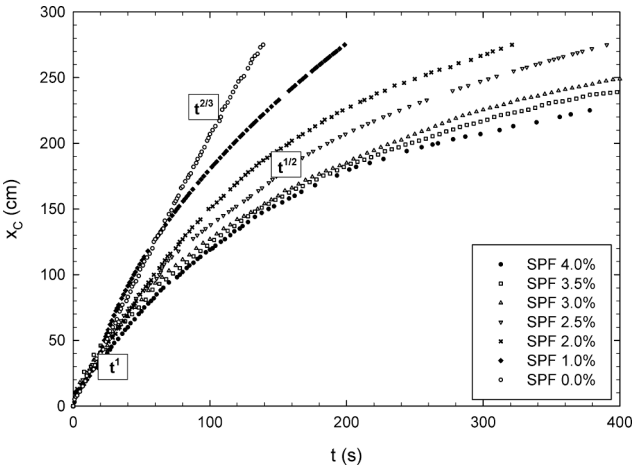

Fig. 3. Temporal evolution of the turbidity current toe for fully-vegetated runs carried out using different vegetation canopy densities and the non-vegetated case.

deceleration was greater in the vegetated runs. The evolution of x_c in Run 6 is shown in Fig. 4A as an example of transition from the inertial regime ($x_c \propto t^1$) to the drag-dominated regime ($x_c \propto t^{1/2}$) and finally to the viscous regime ($x_c \propto t^{1/5}$). The positions at which these regime transitions occurred are referred to hereafter as $x_c = L_{ini}$ (the position at which the current transitions from the inertial regime, and the drag-dominated regime is initiated) and $x_c = L_{end}$ (the position at which the drag-dominated regime ends and the viscous regime begins).

The normalized toe drag was calculated for L_{ini} and L_{end} in each of the fully-vegetated runs. Given that L_{patch}/H was constant across these runs, the relationships of $C_{Da}aL_{ini}$ and $C_{Da}aL_{end}$ to the other independent variable defined above, aH, were investigated, and plotted in Fig. 4B. Both varied linearly with aH for $aH < 0.8$, following

$$C_{Da}aL_{ini} = 7.13aH + 1.32 \quad (2)$$

($r^2 = 0.87$; n = 10; $p < 0.001$) and

$$C_{Da}aL_{end} = 12.24aH + 3.92 \quad (3)$$

($r^2 = 0.97$; n = 10; $p < 0.001$), respectively. When $aH > 0.8$, both were constant at $C_{Da}aL_{ini} = 7.1 \pm 0.2$ and $C_{Da}aL_{end} = 13.1 \pm 0.2$, respectively.

3.2. Turbidity current evolution in finite-length vegetation patch runs

As noted above, values of $C_{Da}aL_{ini}$ and $C_{Da}aL_{end}$ from Run 7 were used to determine the lengths of the vegetation patches in the finite-length patch runs. In Run 7, $aH = 1.02$, so $C_{Da}aL_{ini} \approx 7$ and $C_{Da}aL_{end} \approx 13$. Patch lengths were thus chosen for Runs 16–25 such that $C_{Da}aL_{patch} = 6$, 8, 10, 12 and 14, using each in one run with $H = 12$ cm and another with $H = 6$ cm (Table 2). The $C_{Da}aL_{patch} = 6$ patch (Runs 20 and 25) ended in the inertial regime of Run 7; the $C_{Da}aL_{patch} = 8$, 10 and 12 patches (Runs 17–19 and 22–24) ended in the drag-dominated regime of Run 7; and the $C_{Da}aL_{patch} = 14$ patch (Runs 16 and 21) ended in the viscous regime of Run 7.

In qualitative terms, the evolution of the currents proceeded as expected. In Runs 16 and 21, both L_{ini} and L_{end} occurred within the vegetation, so the current underwent its full evolution and reached the viscous regime within the vegetation, behaving as if in a continuous, infinite-length canopy (Fig. 5C). In runs 17–19 and 22–24, L_{ini} occurred within the vegetation, but the current emerged from the patch in a drag-dominated state and subsequently transitioned to a viscous regime downstream of the patch, apparently without changing to a self-similar state (in which $x_c \propto t^{2/3}$ would have been observed) despite the absence of vegetative drag (Fig. 5B). Here too, therefore, the current behaved as

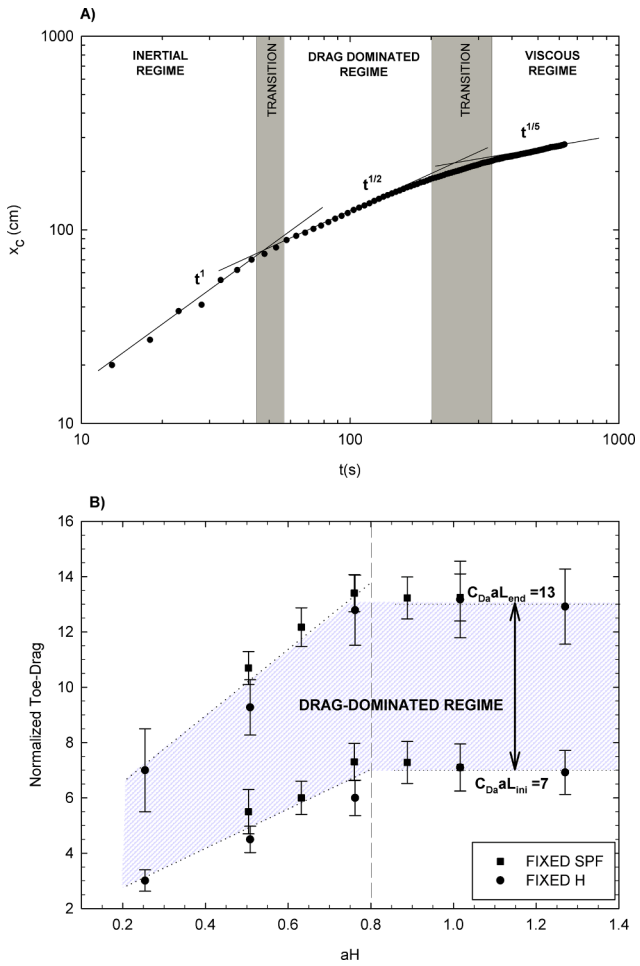

Fig. 4. (A) Plot of the temporal evolution of the turbidity current toe for Run 6 (H = 12 cm, SPF = 3.5%). The three hydrodynamic regimes can be distinguished by their different slopes: 1 for the inertial regime, 1/2 for the drag-dominated regime and 1/5 for the viscous regime. The transition zones between these regimes are indicated by grey zones. (B) Plot of normalised toe drag, $C_{Da}ax_c$, versus the non-dimensional frontal canopy area, aH, showing values at which the drag-dominated regime begins ($C_{Da}aL_{ini}$) and ends ($C_{Da}aL_{end}$). Data are from Runs 2–7 (H = 12 cm, SPF = 1 to 4%) (circles), and from Runs 8–11 (SPF = 4%, H = 3, 6, 9, 12 and 15 cm) (squares). Dashed lines represent the linear best fit of the data. The grey area indicates the drag-dominated regime.

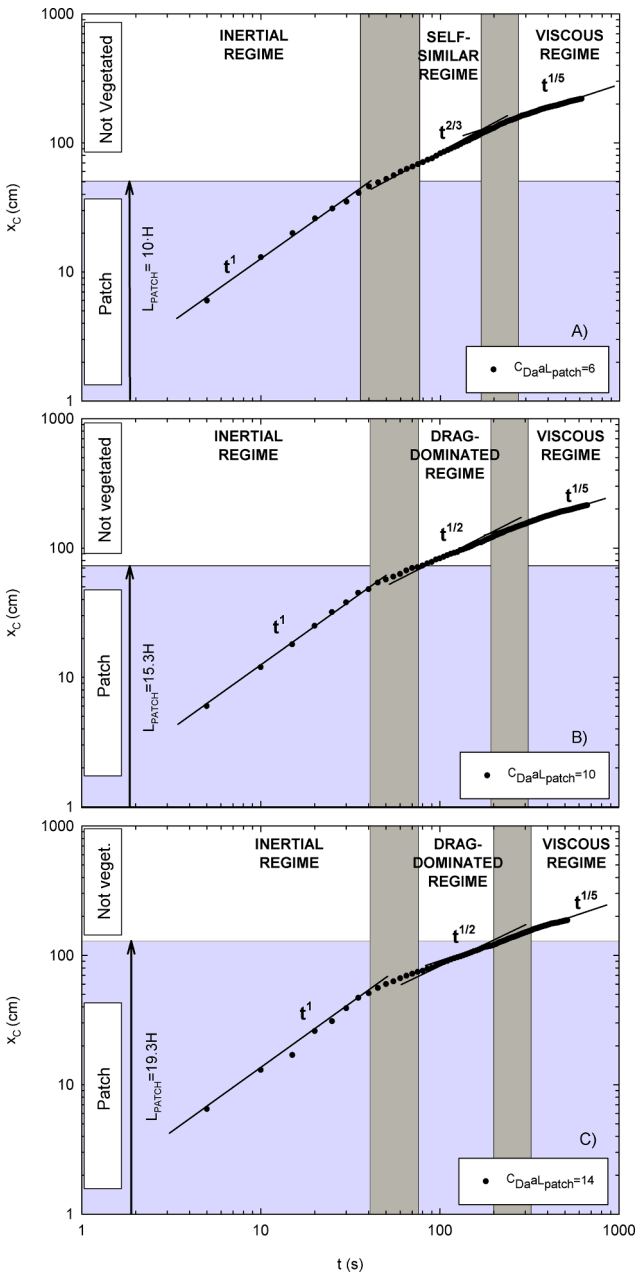

Fig. 5. Plot of the temporal evolution of the current toe position, x_c, for vegetation patches with a water height H = 6 cm, SPF = 4% and a patch length L_{patch} of (A) 60 cm (10H); (B) 92 cm (15.3H, black circles) and (C) 116 cm (19.3H, white circles). The inertial regime ends downstream of the patch in (A), but within it in cases shown in (B) and (C). The three hydrodynamic regimes that the current passes through in each case are shown. Note that in (A) the inertial regime transitions to a self-similar regime ($x_c \propto t^{2/3}$), whereas in (B) and (C) it transitions to a drag-dominated regime ($x_c \propto t^{1/2}$).

if in a fully-vegetated, continuous canopy, transitioning to a drag-dominated state rather than a self-similar state. In runs 20 and 25, the vegetation patch ended upstream of L_{ini}, so the current was still in the inertial regime as it emerged from the patch and evolved as if it were flowing in a non-vegetated flume, passing through self-similar ($x_c \propto t^{2/3}$) and viscous regimes (Fig. 5A).

Quantitatively, and surprisingly, L_{ini} had a consistent relationship with aH and L_{patch}/H, regardless of whether the regime transitions occurred within the patch or downstream of it. This is shown in Fig. 6, in which data from both the fully-vegetated and finite patch runs all fall on a line with both axes in log form, that means there is a power law relationship given by

$$\frac{L_{ini}}{H} = 3.721\left[(aH)^{0.64}\left(\frac{L_{patch}}{H}\right)^{-0.30}\right]^{-0.77} \quad (4)$$

3.3. Sediment deposition from turbidity currents in vegetation patches

We focussed our analysis of sediment deposition on the drag-dominated regime of the currents' evolution. DF values were selected from the sediment trap that was positioned closest to the middle of the drag-dominated region in each run. These were taken to be representative of the sediment deposition across the whole drag-dominated regime and, because that regime occurred in between the inertial and viscous regimes, to be also representative of the sediment deposition from the turbidity current as a whole. As for the hydrodynamic data, the DF values were analysed in relation to aH and L_{patch}/H. The results of this analysis are shown in Fig. 7, in the form of plots of DF/aH against L_{patch}/H. Across all runs, for both fine and coarse particles, DF/aH was approximately constant when $L_{patch}/H < 20 \pm 2$, and increased with

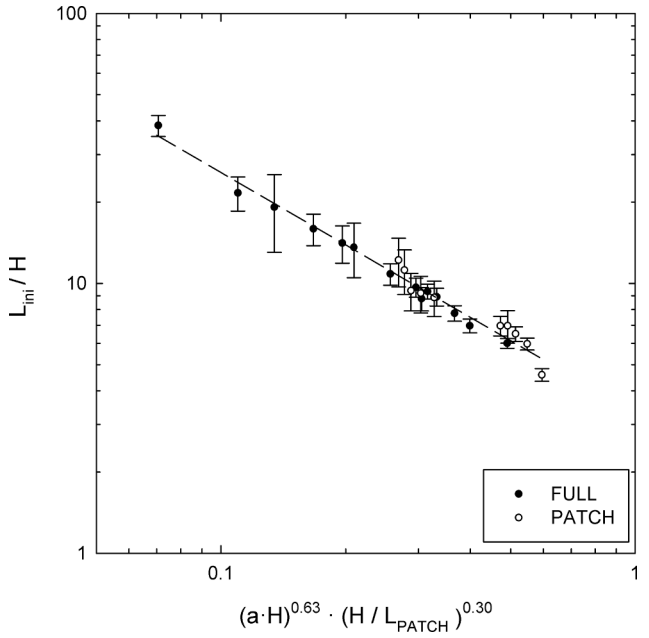

Fig. 6. Plot of the current toe position at which the drag-dominated regime begins, L_{ini}, non-dimensionalized by water height H, against the function of aH and L_{patch}/H shown in Eq. (3). Data from all experimental runs using both fully-vegetated (black circles) and vegetation patch (white circles) configurations are shown. The dashed line illustrates the power best fit ($\sim A \cdot x^B$) of the data with A = 3.72; B = −0.77, $r^2 = 0.95$; n = 23; $p \ll 0.01$.

increasing L_{patch}/H, following a power law relationship, above this threshold value (Fig. 7).

The behaviour of DF differed for coarse and fine particle fractions. For $L_{patch}/H < 20 \pm 2$,

$$DF_{fine} = 0.758aH \quad (5)$$

(n = 24, 95% confidence interval [0.631, 0.885]) for fine sediment and

$$DF_{coarse} = 0.475aH \quad (6)$$

(n = 23, 95% confidence interval [0.359, 0.592]) for coarse sediment. This implies a fine-to-coarse flux ratio, DF_{fine}/DF_{coarse}, of 0.767/0.489 = 1.60. For $L_{patch}/H > 20 \pm 2$, the value of DF/aH increases with increasing patch length for both fine and coarse fractions, i.e. the rate of deposition was greater in these longer patches than it would have been in shorter patches of the same density. But the rate of fine particle deposition continued to be greater than that of coarse particle deposition. This difference reduced towards unity as patch length increased, but only slowly, such that when $L_{patch}/H = 88.5$ (the maximum value used here), it was approximately 1.34.

4. Discussion

4.1. Agreement with previous studies

The time evolution of turbidity currents flowing through different distributions of vegetation were studied. In the non-vegetated control case (Run 1), the particles settling out of the current caused a reduction of its density anomaly as it progressed forward, causing a reduction of the current toe speed. Thus, after the initial inertial regime ($x_c \propto t^1$), the position of the current toe followed the time dependence, $x_c \propto t^{2/3}$, found by Bonnecaze et al. (1993) for the same flow configuration. In the runs in which the turbidity current flowed through continuous vegetation, for all vegetation density and water height combinations tested, the pattern of evolution of the current dynamics was found to be in

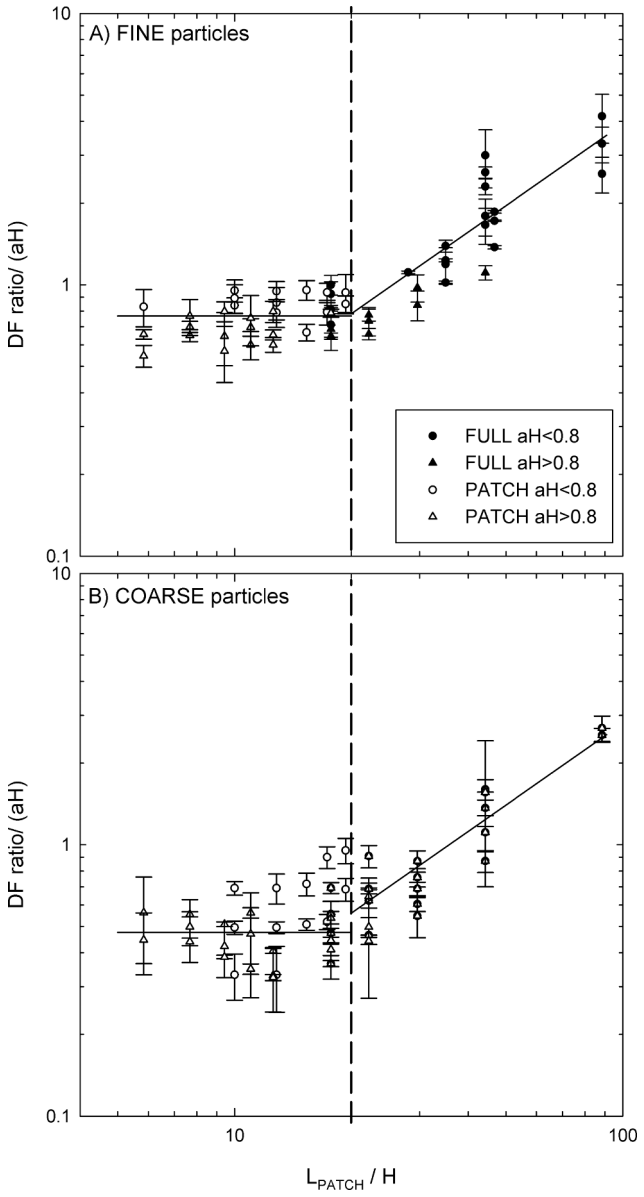

Fig. 7. Ratio of the non-dimensional depositional sediment flux, DF, to the canopy frontal area aH at sediments traps located near the centre of the drag-dominated regime for each run, plotted against the canopy aspect ratio, L_{patch}/H for (A) fine particles and (B) coarse particles. The plots are divided into two zones denoting the difference in behaviour that depends on whether L_{patch}/H is greater or$<20 \pm 2$. The lines illustrate the linear best fits of the data with the right hand sections of each one having: (a) m = 0.039, $r^2 = 0.80$, n = 28, $p \ll 0.01$; and (b) m = 0.022, $r^2 = 0.83$, n = 31, $p \ll 0.01$. Data shown for all runs: fully-vegetated runs with canopy frontal areas, aH, smaller than 0.8 (black circles) and>0.8 (black triangles), and vegetation patch runs with canopy frontal areas smaller than 0.8 (white circles) and>0.08 (white triangles).

agreement with previous studies (Hatcher et al., 2000; Tanino et al., 2005; Zhang and Nepf, 2008). That is, the turbidity current developed initially in the inertial regime, as in the non-vegetated case, but soon transitioned to a drag-dominated regime, where it was further slowed by the vegetation drag, so that the position of the current toe followed $x_c \propto t^{1/2}$, and subsequently reached a viscous regime where $x_c \propto t^{1/5}$. Soler et al. (2020) found that turbidity currents in *Arthrocnemum fruticosum* (semi rigid) and *Ruppia maritima* (flexible) vegetation beds behave like in beds covered by rigid stems of PVC. Therefore, the results here found, are expected to apply in the development of turbidity currents through real patches of vegetation. The flexibility of vegetation did not

determine the fate of gravity currents within vegetation, rather the frontal plant obstruction provided by the vegetation. Furthermore, less dense turbidity currents ($C_o = 1$ g·L^{-1} and Co = 3 g·L^{-1}) would not give different results either (Soler et al., 2020).

4.2. Effects of water depth on regime transition positions

Unlike previous studies (Soler et al., 2017, 2020), the experiment reported here investigated the effect on turbidity currents of varying water depth as well as canopy density. This revealed that there is a threshold value of the non-dimensional parameter aH, above which the non-dimensionalized positions at which turbidity currents transition from being inertially-dominated to drag-dominated ($C_{Da}aL_{ini}$), and subsequently from being drag-dominated to dominated by viscous forces ($C_{Da}aL_{end}$), are constant. This threshold value was found to be $aH = 0.8$, above which $C_{Da}aL_{ini} = 7.1 \pm 0.2$, and $C_{Da}aL_{end} = 13.1 \pm 0.2$. The former agrees with Tanino et al. (2005) and Soler et al. (2020), who found that $C_{Da}aL_{ini} \approx 7$ remained the case up to $aH = 2.3$, compared to a maximum value of 1.27 in this study. When $aH < 0.8$, both $C_{Da}aL_{ini}$ and $C_{Da}aL_{end}$ decreased linearly with decreasing aH. This is consistent with an explanation that considers the relative influence of drag forces due to the canopy elements compared to other drag forces, including those due to bed shear stress and interfacial stresses between the turbidity current and its overflowing counter current. Note, first, that small values of aH imply vegetation canopies that are either sparse or in shallow water, or both. In shallow water, sparse canopy cases, the drag forces not due to the canopy will have relatively significant influence, meaning that drag forces are greater than predicted by models that only consider the canopy drag (such as that formulated by Tanino et al., 2005, who originally devised the normalised toe drag parameter) and therefore regime transitions will happen earlier than predicted by those models, as found here. If either canopy density or water depth are increased, the non-canopy drag forces become less significant, so the canopy drag-based model fits the data better. Our findings, as illustrated in Fig. 4B, suggest that this effect is manifested in the change of relationship at $aH = 0.8$ shown.

4.3. Patch length vs. Regime transition distances

From the empirical relationship found in these data between L_{ini}/H, aH and L_{patch}/H (Equation (4)), setting $L_{ini} \leq L_{patch}$ gives

$$L_{patch} \geq 5.51 a^{-0.636} H^{0.364} \tag{7}$$

This inequality gives the patch lengths for which the transition to the drag-dominated regime will occur within a vegetated patch, and thus the patch length required to have the same effect on the position of turbidity currents' transition to the drag-dominated regime as a continuous vegetation canopy. From (7), this patch length is only weakly dependent on H and close to being directly proportional to the reciprocal of a. If L_{patch} is shorter than this threshold, the current will emerge from the patch still in its inertial regime and therefore transition to a self-similar regime rather than a drag-dominated one.

Thus, the results presented here corroborate previous findings that denser canopies cause turbidity currents to transition earlier into the drag-dominated regime (Barcelona et al., 2018). If the vegetated patch is denser (increased a), the turbidity current experiences higher vegetative drag and consequently a smaller patch length is required to cause this transition. To give some indications of the threshold patch length scales that our results imply, sparse patches (say, $a = 2$ m^{-1}) developing in shallow water, with a characteristic depth of, say, 10 cm, need to be at least 1.54 m in length to cause turbidity currents to transition to a drag-dominated state in the same way as a continuous canopy would, while in denser patches (say, a = 10 m^{-1}) in the same water depth, a patch length of 0.55 m would be enough for this to occur. In deeper water (say, H = 1 m), the same sparse patches would need to have a length of 3.54 m to cause the transition at the same point as a continuous canopy, while in the same denser patches the required length would be 1.26 m. For exemplar, common saltmarsh species *Arthrocnemum fruticosum* (glasswort) and *Juncus maritimus* (sea rush), for which canopy densities of a = 3.64 m^{-1} and 4.69 m^{-1} have been reported respectively (Soler et al., 2020), in water of 0.5 m depth, the threshold patch lengths would be 1.88 m and 1.60 m, respectively. These patch lengths are all of the same order of magnitude as the typical size of patches of vegetation found in salt marsh pioneer zones and seagrasses.

4.4. Sedimentation patterns from turbidity currents in degraded vegetation canopies

Soler et al. (2020) found that, when turbidity currents flow through fully vegetated canopies, coarse particles initially settle faster than fine particles, leaving the finer particles to be dominant in the material deposited in canopy interiors, thus 'muddifying' them. In agreement with this, here we find the rate of fine particle deposition is higher than the rate of coarse particle deposition once the current has entered significantly into the vegetation and transitioned to a drag-dominated state (Fig. 7). At patch lengths such that $L_{patch}/H < 20 \pm 2$, the ratio of fine to coarse deposition rates is constant with respect to L_{patch}/H at $DF_{fine} = 1.60DF_{coarse}$. Above this threshold, the ratio changes, but only slightly. Keeping in mind that the distribution of patches is often affected by geology and topography, these fine sediments, which are often enriched in nutrients (Vandenbruwaene et al., 2011) will result in a positive feed-back, as evidenced by previous observations. For example, Di Carlo et al. (2005) found that in shallow, well-lit waters, seagrass establishment was densest in nutrient-rich sediments zones and Nardin et al. (2016) found mangroves in Mekong delta expanded as continuous coverage in areas of high sediment availability, but as sparse patches in areas of low sediment supply. Thus, this process will favour a shaping of the landscape-scale canopy structure into patches growing on relatively nutrient-rich, fine sediment, separated by gaps with relatively coarse, nutrient-poor sediment. This is redolent of the structure observed in, for example, chalk streams occupied by patches of *Ranunculus* (Cotton et al., 2006), where the flow carrying the sediment is driven by the component of gravity forcing it down the longitudinal slope of the stream channel, rather than the buoyancy forces driving the turbidity currents studied here.

Studies on the role of patch size in the ecosystem engineering capacity of submerged plants have also found that patch size affects patterns of sedimentation within them. Schoelynck et al. (2012) used mimic and transplantation experiments in a small river to show that the longer patches were, the more effectively they slowed the current, enhancing sedimentation. Licci et al. (2019) showed that there is a threshold length that river vegetation patches need to attain in order to induce modifications to flow and sedimentation patterns, and that this threshold value differs depending on environmental conditions such as flow velocity. At low velocity sites (0.13 ± 0.01 ms^{-1}), they found that a patch with a length >0.3 m modified the flow, while at high velocity sites (0.20 ± 0.01 ms^{-1}), the threshold patch length was 0.9 m. They also found fine sediment accumulation within patches was dependent on the velocity of the ambient flow field, which coincides with results of Barcelona et al. (2018). In longitudinal patches the threshold value for having the hydrodynamics and sedimentation affected by fragmentation is related to the fractional volume occupied by vegetation which has to be higher than 0.025 (Barcelona et al., 2018). Licci et al. (2019) results contrast with laboratory flume experiments carried out by Tinoco and Coco (2014) who studied the effect of emergent vegetation on sediment resuspension under uni-directional currents and waves showing that denser vegetated patches, even at low speeds (their lowest speed value was of 8 cm/s), generated turbulence that provoked sediment scour and suspension. In our experiments, the turbidity currents developed frontal velocities with maximum values of 5 cm/s in high density vegetated canopies, for which Re<200 (the threshold value required for vortices to

shed from the dowel (Nepf et al., 1997)) which corroborates Licci et al. (2019) relationship between sediment patterns and patch length, as deposited sediment increased as the length of the patches increased, and extends it to turbidity currents as well as the river flow studied by Schoelynck et al. (2012) and Licci et al. (2019). Our experiments also support the theory that normalized depositional flux rates of sediment are greater in dense patches than in sparse ones, regardless of particle size. Zhang et al. (2020) also found, in field studies in the floodplain of Dongting Lake (China), that the presence of vegetation was more beneficial to the deposition of suspended sediment within vegetation, where the reduction of mean velocity and TKE compared with bare bed resulted in a decrease of 30–50% of suspended sediment concentration, and an increase as high as 190% in sediment deposition compared to bare beds at the same region. In the context of turbidity currents, a threshold value has been found, such that for patches smaller than 20 ± 2 times the water depth, dependency with patch length disappears and sediment deposition rates depend only on the vegetation density.

5. Conclusions

Laboratory flume experiments have been reported which, for the first time, investigate (a) the effects of varying water depth on the passage of turbidity currents through continuous arrays of obstacles; and (b) the effects of finite-length arrays of obstacles on the hydrodynamics and patterns of sediment deposition of turbidity currents, compared to those of continuous, quasi-infinite obstacle arrays. Our interest lies primarily in contexts where the obstacle arrays are aquatic vegetation canopies, but they can equally be taken to simulate other natural or built phenomena. The patch lengths studied were of the same order of magnitude as the length scales over which the turbidity currents develop and decay, allowing the influence of patches on these processes to be elucidated. We varied patch length, canopy density and water height, but did not vary either the initial sediment concentration of the turbidity current fluid, or the physical properties of the material used to simulate the canopy vegetation, so the reported findings do not speak to the possible effects of these last two factors.

We found that the influence of the vegetation patches on turbidity currents is parameterised by two non-dimensional variables: the canopy's frontal area density, aH, and the patch's aspect ratio with respect to the water depth, L_{patch}/H. We found strong relationships between these two parameters and (i) the downstream distances at which the currents transition from an inertial regime to a drag-dominated regime; and (ii) the rate of depositional sediment flux from the current to the bed, and the ratio of values of this flux for fine and coarse sediment fractions. The transition distances, normalized by water depth, are found to follow a power law relationship with aH and L_{patch}/H, which is independent of the dynamical state of the current at the point where it emerges from the patch. The depositional flux rates for fine and coarse sediment fractions, normalised by the canopy density, DF/aH, are both found to be constant for $L_{patch}/H < 20 \pm 2$, with the value for fine sediment greater than that for coarse sediment by a factor of 1.60. For $L_{patch}/H > 20 \pm 2$, the value of DF/aH increases with L_{patch}/H, i.e. the rate of deposition is greater for any given canopy density than it would be in patches shorter than $20 \pm 2H$. If we consider vegetation canopy density values typically found in nature and typical shallow water depths of order 0.1–1 m, the patch sizes at which these thresholds in influence occur are of the order of tens of centimetres to a few metres, which are typical sizes of vegetation patches found in many freshwater and coastal marine contexts. Thus, the results presented here are highly relevant to understanding the interactions of turbidity currents with vegetation in natural environments, and in turn to obtain insights into vegetation–flow–sediment interactions which are crucial for river and wetland management and ecological restoration.

CRediT authorship contribution statement

Marianna Soler: Conceptualization, Data acquisition, Formal analysis. **Teresa Serra:** Conceptualization, Formal analysis. **Andrew Folkard:** Formal analysis. **Jordi Colomer:** Conceptualization, Formal analysis.

Declaration of Competing Interest

The authors declare that they have no known competing financial interests or personal relationships that could have appeared to influence the work reported in this paper.

Acknowledgments

This project has been funded by the University of Girona through grant MPCUdG2016-006 and by the Ministerio de Economía, Industria y Competitividad of the Spanish Government through the grant CGL2017-86515-P.

References

Adam, P., 2002. Saltmarshes in a time of change. Environ. Conserv. 29, 39–61.
Adhitya, A., Bouma, T.J., Folkard, A.M., van Katwijk, M.M., Callaghan, D.P., de Iongh, H. H., Herman, P.M.J., 2014. Comparison of the influence of patch-scale and meadow-scale characteristics on flow within seagrass meadows: A flume study. Mar. Ecol. Prog. Ser. 516, 49–59.
Agawin, N.S.R., Duarte, C.M., 2002. Evidence of direct particle trapping by a tropical seagrass meadow. Estuaries Coasts 25, 1205–1209. https://doi.org/10.1007/BF02692217.
Barcelona, A., Serra, T., Colomer, J., University of Girona, 2018. Fragmented canopies control the regimes of gravity current development. J. Geophys. Res.: Oceans 123, 1631–1646. https://doi.org/10.1002/2017JC013145.
Benjamin, T.B., 1968. Gravity currents and related phenomena. J. Fluid Mech. 31, 209–248.
Bhaganagar, K., 2014. Direct numerical simulation of lock-exchange density currents over the rough wall in slumping phase. J. Hydraul. Res. 52, 386–398.
Blott, S.J., Pye, K., 2012. Particle size scales and classification of sediment types based on particle distributions: review and recommended procedures. Sedimentology 59, 2071–2096.
Bonnecaze, R.T., Huppert, H.E., Lister, J.R., 1993. Particle-driven gravity currents. J. Fluid Mech. 250, 339–369.
Bouma, T.J., Van Duren, L.A., Temmerman, S., Claverie, T., Blanco-Garcia, A., Ysebaert, T., Herman, P.M.J., 2007. Spatial flow and sedimentation patterns within patches of epibenthic structures: Combining field, flume and modelling experiments. Cont. Shelf Res. 27, 1020–1045.
Bouma, T.J., Friedrichs, M., Van Wesenbeeck, B.K., Temmerman, S., Graf, G., Herman, P. M.J., 2009. Density-dependent linkage of scale-dependent feedbacks: A flume study on the intertidal macrophyte *Spartina anglica*. Oikos 118, 260–268. https://doi.org/10.1111/j.1600-0706.2008.16892.x.
Bouma, T.J., Temmerman, S., Van Duren, L.A., Martini, E., Vandenbruwaene, W., Callaghan, D.P., Balke, T., Biermans, G., et al., 2013. Organism traits determine the strength of scale-dependent bio-geomorphic feedbacks: A flume study on three intertidal plant species. Geomorphology 180–181, 57–65.
Colomer, J., Soler, M., Serra, T., Casamitjana, X., Oldham, C., 2017. Impact of anthropogenically created canopy gaps on wave attenuation in a *Posidonia oceanica* seagrass meadow. Mar. Ecol. Prog. Ser. 569, 103–116.
Cotton, J., Wharton, G., Bass, J., Heppell, C., Wotton, R., 2006. The effects of seasonal changes to in-stream vegetation cover on patterns of flow and accumulation of sediment. Geomorphology 77, 320–334.
Curran, J.C., Hession, W.C., 2013. Vegetative impacts on hydraulics and sediment processes across the fluvial system. J. Hydrol. 505, 364–376.
Di Carlo, G., Badalamenti, F., Jensen, A.C., Koch, E.W., Riggio, S., 2005. Colonisation process of vegetative fragments of *Posidonia oceanica* (L.) Delile on rubble mounds. Mar. Biol. 147, 1261–1270. https://doi.org/10.1007/s002277-005-0035-0.
Dwirea, K.A., Mellmann-Brown, S., Gurrieri, J.T., 2018. Potential effects of climate change on riparian areas, wetlands, and groundwater-dependent ecosystems in the Blue Mountains, Oregon, USA. Clim. Serv. 10, 44–52.
El Allaoui, N., Serra, T., Soler, M., Pujol, D., Oldham, C., 2015. Modified hydrodynamics in canopies with longitudinal gaps exposed to oscillatory flows. J. Hydrol. 531, 840–849.
El Allaoui, N., Serra, T., Colomer, J., Soler, M., Casamitjana, X., Oldham, C., 2016. Interactions between fragmented seagrass canopies and the local hydrodynamics. PLoS ONE 11, 5. https://doi.org/10.1371/journal.pone.0156264.
Felix, M., 2002. Flow structure of turbidity currents. Sedimentology 49, 397–419.
Folkard, A.M., 2005. Hydrodynamics of model *Posidonia oceanica* patches in shallow water. Limnol. Oceanogr. 50, 1592–1600. https://doi.org/10.4319/lo.2005.50.5.1592.

Folkard, A.M., 2019. Biophysical interactions in fragmented canopies: Fundamental processes, consequences, and upscaling. Front. Mar. Sci. 6 https://doi.org/10.3389/fmars.2019.00279.
Francisco, E.P., Espath, L.F.R., Laizet, S., Silvestrini, J.H., 2017. Reynolds number and settling velocity influence for finite-release particle-laden gravity currents in a basin. Comput. Geosci. 110, 1–9.
Ghisalberti, M., Nepf, H.M., 2004. The limited growth of vegetated shear layers. Water Resoures. Res. 40, W07502. https://doi.org/10.1029/2003WR002776.
Gillis, L.G., Maza, M., Argemi, M., Balke, T., Folkard, A.M., Garcia-Maribona, J., Geng, L., Lanzoni, S., Meire, D., Paul, M., Sgarabotto, A., Suzuki, T., Lara, J.L., 2019. Plant effects on hydrodynamics and sedimentation at coastal wetland edges. Proceedings of the HYDRALAB+ Joint User Meeting.
Gladstone, C., Phillips, J.C., Sparks, R.S.J., 1998. Experiments on bidisperse, constant-volume gravity currents: propagation and sediment deposition. Sedimentology 45, 833–843.
Gonzalez-Juez, E., Meiburg, E., Tokyay, T., Constantinescu, G., 2010. Gravity current mixing in gravity currents propagating up mild slopes flow past a circular cylinder: Forces, wall shear stresses and implications for scour. J. Fluid Mech. 649, 69–102.
Gurnell, A., 2014. Plants as river system engineers, Earth Surf. Process. Landforms. 39, 4–25.
Harris, T.C., Hogg, A.J., Huppert, H., 2002. Polydisperse particle-driven gravity currents. J. Fluid Mech. 472, 333–371.
Harvey, J.W., Schaffranek, R.W., Noe, G.B., Larsen, L.G., Nowacki, D.J., O'Connor, B.L., 2009. Hydroecological factors governing surface water flow on a low-gradient floodplain. Water Resour. Res. 45 https://doi.org/10.1029/2008WR007129.
Hatcher, L., Hogg, A.J., Woods, A.W., 2000. The effect of drag on turbulent gravity currents. J. Fluid Mech. 416, 297–314.
Huppert, H.E., Simpson, J.E., 1980. The slumping of gravity currents. J. Fluid Mech. 99, 785–799.
Joensuu, M., Pilditch, C.A., Harris, R., Hietanen, S., Pettersson, H., Norkko, H.A., 2018. Sediment properties, biota, and local habitat structure explain variation in the erodibility of coastal sediments. Limnol. Oceanogr. 63, 173–186.
La Rocca, M., Adduce, C., Sciortino, G., Pinzon, A.B., 2008. Experimental and numerical simulation of three-dimensional gravity currents on smooth and rough bottom. Phys. Fluids 20, 106603. https://doi.org/10.1063/1.3002381.
Leonard, L.A., Hine, A.C., Luther, M.E., 1995. Surficial sediment transport and deposition processes in Juncus Romerianus marsh, West-Central Florida. J. Coastal Res. 11, 322–326.
Licci, S., Nepf, H., Delolme, C., Marmonier, P., Bouma, T.J., Puijalon, S., 2019. The role of patch size in ecosystem engineering capacity: A case study of aquatic vegetation. Aquat. Sci. 81, 41. https://doi.org/10.1007/s00027-019-0635-2.
Liu, C., Nepf, H., 2015. Sediment deposition within and around a finite patch of model vegetation over a range of channel velocity. Water Resour. Res. 52, 600–612. https://doi.org/10.1002/2015WR018249.
Lowe, B.J., Watts, R.J., Roberts, J., Robertson, A., 2010. The effect of experimental inundation and sediment deposition on the survival and growth of two herbaceous riverbank plant species. Plant Ecol. 2010 (209), 57–69. https://doi.org/10.1007/s11258-010-9721-1.
Ludwig, J.A., Wilcox, B.P., Breshears, D.D., Tongway, D.J., Imeson, A.C., 2005. Vegetation patches and runoff-erosion as interacting ecohydrological processes in semiarid landscapes. Ecology 86 (2), 288–297.
Madsen, J.D., Chambers, P.A., James, W.F., Koch, E.W., Westlake, D.F., 2001. The interaction between water movements, sediment dynamics and submersed macrophytes. Hydrobiologia 444, 71–84.
Mandal, S., Maiti, R., 2015. Semi-quantitative Approaches for Landslide Assessment and Prediction. Springer Natural Hazards. Berlin, Springer.
Manners, R.B., Wilcox, A.C., Kui, L., Lightbody, A.F., Stella, J.C., Sklar, L.S., 2015. When do plants modify fluvial processes ? Plant-hydraulic interactions under variable flow and sediment supply rates. J. Geophys. Res. Earth Surf. 120, 325–345. https://doi.org/10.1002/2014jf003265.
Maxworthy, T., Leilich, J., Simpson, J.E., Meiburg, E.H., 2002. The propagation of a gravity current in a linearly stratified fluid. J. Fluid Mech. 453, 371–394.
Meiburg, E., Kneller, B., 2010. Turbidity Currents and Their Deposits. Ann. Rev. Fluid Mech. 42 (1) https://doi.org/10.1146/annurev-fluid-121108-145618.
Montakhab, A., Yusuf, B., Ghazali, A.H., Mohamed, T.A., 2012. Flow and sediment transport in vegetated waterways: A review. Rev. Environ. Sci. Biotechnol. 11, 275–287.
Nardin, W., Locatelli, S., Pasquarella, V., Rulli, M.C., Woodcock, C.E., Fagherazzi, S., 2016. Dynamics of a fringe mangrove forest detected by landsat images in the Mekong river delta, Vietnam. Earth Surf. Process. Landf. 41, 2024–2037. https://doi.org/10.1080/00221686.2012.696559.
Nepf, H.M., 1999. Drag, turbulence, and diffusion in flow through emergent vegetation. Water Resour. Res. 35 (2), 479–489.
Nepf, H.M., 2012. Flow and transport in regions with aquatic vegetation. Annu. Rev. Fluid Mech. 44, 123–142. https://doi.org/10.1146/annurev-fluid-120710-101048.
Nepf, H.M., Mugnier, C.G., Zavistoski, R.A., 1997. the Effects of Vegetation on Longitudinal Dispersion. Estuar. Coast. Shelf Sci. 44 (6), 675–684. https://doi.org/10.1006/ecss.1996.0169.
Nogueira, H.I.S., Adduce, C., Alves, E., Franca, M.J., 2013. Analysis of lock-exchange gravity currents over smooth and rough beds. J. Hydraul. Res. 51 (4), 417–431.
Nogueira, H.I.S., Adduce, C., Alves, E., Franca, M.J., 2014. Dynamics of the head of gravity currents. Environ. Fluid. Mech. 14, 519–540.
Pujol, D., Colomer, J., Serra, T., Casamitjana, X., 2010. Effect of submerged aquatic vegetation on turbulence induced by an oscillating grid. Cont. Shelf Res. 30, 1019–1029.
Pujol, D., Serra, T., Colomer, J., Casamitjana, X., 2013. Flow structure in canopy models dominated by progressive waves. J. Hydrology 486, 281–292.
Richardson, D.M., Holmes, P.M., Esler, K.J., Galatowitsch, S.M., Stromberg, J.C., Kirkman, S.P., Pysek, P., Hobbs, R.J., 2007. Riparian vegetation: Degradation, alien plant invasions, and restoration prospects. Divers. Distrib. 13, 126–139.
Rietkerk, M., van de Koppel, J., 2008. Regular pattern formation in real ecosystems. Trends Ecol. Evol. 23, 169–175.
Schoelynck, J., De Groote, T., Bal, K., Vandenbruwaene, W., Meire, P., Temmerman, S., 2012. Self-organised patchiness and scale-dependent bio-geomorphic feedbacks in aquatic river vegetation. Ecography 35, 760–768. https://doi.org/10.1111/j.1600-0587.2011. 07177.x.
Schulze, D., Rupprecht, F., Nolte, S., Jensen, K., 2019. Seasonal and spatial within-marsh differences of biophysical plant properties: Implications for wave attenuation capacity of salt marshes. Aquat. Sci. 81 (4) https://doi.org/10.1007/s00027-019-0660-1.
Serra, T., Colomer, J., Gacia, E., Soler, M., Casamitjana, X., 2002. Effects of a turbid hydrothermal plume on the sedimentation rates in a karstic lake. Geophys. Res. Lett. 29 https://doi.org/10.1029/2002GL015368.
Serra, T., Soler, M., Julia, R., Casamitjana, X., Colomer, J., 2005. Behaviour and dynamics of a hydrothermal plume in Lake Banyoles, Catalonia, NE Spain. Sedimentology 52, 795–808.
Serra, T., Colomer, J., Oldham, C., 2018. Local hydrodynamics at edges of marine canopies under oscillatory flows. PLoS One 13, 8. https://doi.org/10.1371/journal.pone.0201737.
Shin, J.O., Dalziel, S.B., Linden, P.F., 2004. Gravity currents produced by lock exchange. J. Fluid Mech. 521, 1–34. https://doi.org/10.1017/S002211200400165X.
Simpson, J.E., 1982. Gravity currents in the laboratory, atmosphere, and ocean. Annu. Rev. Fluid Mech. 14, 213–234.
Soler, M., Colomer, J., Serra, T., Casamitjana, X., Folkard, A.M., 2017. Sediment deposition from turbidity currents in simulated aquatic vegetation canopies. Sedimentology 64, 1132–1146.
Soler, M., Colomer, J., Folkard, A.M., Serra, T., 2020. Particle size segregation of turbidity current deposits in vegetated canopies. Sci. Total Environ. https://doi.org/10.1016/j.scitotenv.2019.134784.
Tamburello, L., Benedetti-Cecchi, L., Ghedini, G., Alestra, T., Bulleri, F., 2012. Variation in the structure of subtidal landscapes in the NW Mediterranean Sea. Mar. Ecol. Prog. Ser. 457, 29–41.
Tanino, Y., Nepf, H.M., Kulis, P.S., 2005. Gravity currents in aquatic canopies. Water Resour. Res. 41, W12402. https://doi.org/10.1029/2005WR004216.
Tinoco, R.O., Coco, G., 2014. Observations of the effect of emergent vegetation on sediment resuspension under unidirectional currents and waves. Earth Surf. Dyn. 2, 83–96. https://doi.org/10.5194/esurf-2-83-2014.
Van Rijn, L.C., 2007. Unified view of sediment transport by currents and waves I: Initiation of motion, bed roughness, and bed-load transport. J. Hydraul. Eng. 133, 649–667.
Vandenbruwaene, W., Temmerman,S., Bouma, T.J., Klaassen, P.C., de Vries, M.B., Callaghan, D.P., van Steeg, P., Dekker, F. van Duren, L.A., Martini, E. , T. Balke, T., Biermans, G.
White, F.M., 1991. Viscous Fluids Flow, 2nd ed. McGraw-Hill, New York.
Xiu, L., Yan, C., Li, X., Qian, D., Feng, K., 2019. Changes in wetlands and surrounding land cover in a desert area under the influences of human and climatic factors: A case study of the Hongjian Nur region. Ecol. Ind. 101, 261–273.
Zhang, Y., Lai, X., Zhang, L., Song, K., Yao, X., Gu, L., Pang, C., 2020. The influence of aquatic vegetation on flow structure and sediment deposition: A field study in Dongting Lake, China. J. Hydrol. 584 https://doi.org/10.1016/j.jhydrol.2020.124644.
Zhang, X., Nepf, H.M., 2008. Density-driven exchange flow between open water and aquatic canopy. Water Resour. Res. 44, W08417. https://doi.org/10.1029/2007WR006676.
Zhang, X., Nepf, H.M., 2011. Exchange flow between open water and floating vegetation. Environ Fluid Mech. 11, 531–546.
Zhang, X., Tang, C., Nepf, H.M., 2018. Turbulent kinetic energy in submerged model canopies under oscillatory flow. Water Resour. Res. 54 https://doi.org/10.1002/2017WR021732.
Zong, L., Nepf, H.M., 2010. Flow and deposition in and around a finite patch of vegetation. Geomorphology 116, 363–372. https://doi.org/10.1016/j.geomorph.2019.11.020.